Morphology and immersion behavior of plasma-sprayed hydroxyapatite/bioactive glass coatings

S. J. DING, C. P. JU, J. H. CHERN LIN
Department of Materials Science and Engineering, National Cheng Kung University, Tainan, Taiwan, R.O.C.

A series of hydroxyapatite/bioactive glass (HA/BG) coatings have been plasma-sprayed on Ti6Al-4V substrate using HA/BG powders that were prepared by both sinter-granulation and direct mixing methods. The morphology and immersion behavior of these coatings in a simulated body fluid (SBF) were investigated. The results showed that in-house fabricated BG and sinter-granulated HA powders were irregularly shaped and dense. When 5 wt % or more BG was added in HA, the powder became rough and porous. X-ray diffraction (XRD) patterns showed that the presence of BG enhanced the decomposition of HA structure during fabrication of the powders. Reasonably high bond strengths were obtained from all coatings. The granulated type HA/BG coatings showed no significant differences in bond strength from the mixed type HA/BG coatings. The plasma spray process itself and the presence of BG enhanced the decomposition of apatite. Surface morphology of all sinter-granulated type coatings was similar to that of monolithic HA coating, that was comprised of patches of smooth and shiny glassy film and irregularly-shaped particles on its surface. The dissolution depth of plasma-sprayed coatings immersed in SBF was largely dependent on the type and composition of the coating. Granulated type HA/BG coatings were much less dissolvable than monolithic HA or mixed type HA/BG coatings. It seems that the presently used granulation method for the preparation of HA/BG powders plays a predominant role in determining the dissolution behavior of the plasma-sprayed coatings.

1. Introduction

Due to its favorable biocompatibility and mechanical properties, hydroxyapatite (HA)-coated Ti6Al-4V alloy has been accepted as one of the most promising implant materials for orthopedic and dental applications [1–3]. Various deposition techniques, such as dip coating-sintering, immersion coating, hot isostatic pressing (HIP), ion plating, sputtering, pulsed laser deposition and plasma spray, have been explored [4–9]. Among the many techniques, plasma spray is perhaps most popularly used due to its process feasibility as well as reasonably high coating bond strength and mechanical properties.

Several attempts have been made to improve the performance (e.g. bioactivity [10] and mechanical properties) of bulk HA by incorporating bioactive glass (BG) or other second phase particles into HA. For example, Mochida *et al.* [11] developed an apatite-bioactive glass composite (ABC) material by sintering the mixture of HA and 45SF1/4 bioactive glass. The composition of 45SF1/4 was similar to that of 45S5 Bioglass except that 6.7 mol% CaO in 45S5 Bioglass was substituted with CaF_2. Due to the high temperature (1000 °C) interaction between the BG and HA phases, the incorporation of HA into 45SF1/4 caused the glass phase to crystallize.

Knowles and co-workers [12, 13] found that phase transformations of HA into $Ca_5(PO_4)_2SiO_4$, $\alpha - Ca_3(PO_4)_2(\alpha - TCP)$ and $\beta - Ca_3(PO_4)_2(\beta - TCP)$ took place when small amounts (up to 5 wt %) of phosphate-based glasses were added. Such transformations were more profound in the HA containing soda type glass $(Na_2O - P_2O_5)$ than that containing lime type glass $(CaO - P_2O_5)$. A strengthening effect was observed when 2.5 wt % $CaO - P_2O_5$ glass was added in the HA resulting in an HA/α-TCP sintered body. In their study of thermal stability of sintered HA-doped glass $(SiO_2 - CaO - Na_2O - P_2O_5 - Al_2O_3 - B_2O_3)$. Kangasniemi *et al.* [14] showed that, when sintered at temperatures higher than 700 °C, sodium ions diffused into doped HA particles inducing the phase transformation of HA into $NaCaPO_4$. These phase transformations led to changes in properties of the glass.

Chern Lin *et al.* [15, 16] studied a series of HA/BG composite coatings plasma-sprayed on Ti-6Al-4V substrate. The powders used for plasma spray were prepared by directly mixing in-house fabricated BG powder and a commercial HA powder. Their results showed that HA/BG composite coatings were generally more resistant to moisture attack than monolithic HA coating in terms of bond strength degradation. The same authors also found that the presence of HA accelerated the dissolution of BG in Hank's solution. After 10 days of immersion, small

spherical apatite particles of 2–5 μm in diameter were readily formed throughout the composite coating surfaces [17]. In the present study, a series of HA/BG coatings have been plasma-sprayed on Ti-6Al-4V substrate using HA/BG powders that were prepared by both sinter-granulation and direct mixing methods. The morphology and immersion behavior of these coatings in a simulated body fluid (SBF) were investigated.

2. Material and methods

A commercial HA powder (Merck A.G., Darmstadt, Germany) with particle size < 1 μm was used in this study. The composition of this powder is listed in Table I. The in-house fabricated BG used in this study contained frits of SiO_2, Na_2O, CaO and P_2O_5 ($SiO_2 : Na_2O : CaO : P_2O_5 = 10 : 3 : 5 : 2$ in wt.). In preparing the BG, appropriate amounts of the frits were mixed and melted at 1350 °C for two hours. The melt was then quenched in water and fractured fragments of the glass were collected. The fragments were ball milled and sieved to obtain particles with sizes between 44 and 149 μm, a particle size range recommended by the manufacturer of the plasma spray system. Detailed description of the fabrication of the BG powder has been given in an earlier paper [16].

The HA/BG powders with BG contents up to 25 wt % were prepared using both direct mixing and sinter-granulation methods. The sinter-granulation method involved mixing and ball-milling appropriate amounts of HA and BG powders in ethyl alcohol, followed by drying and sintering at 1300 °C for 24 h. The sintered granules were then crushed, milled and sieved to obtain particles with sizes 44–149 μm. In the direct mixing method, the sinter-granulated HA powder was directly mixed with BG powder in a ball mill for 24 h to insure homogeneity of the mixture. Throughout this study the directly mixed HA/BG powders and the plasma-sprayed coatings produced from such powders were designated ''M'' series of powders and coatings, respectively. The sinter-granulated powders and the plasma-sprayed coatings produced from such powders were designated ''G'' series of powders and coatings, respectively. For example, the ''MHA/25BG'' powder stands for the directly mixed powder containing 75 wt % HA and 25 wt % BG, while the ''GHA/10BG'' coating stands for the plasma-sprayed coating from the sinter-granulated powder containing 90 wt % HA and 10 wt % BG.

Commercially available cylindrical rods and plates of Ti-6Al-4V alloy were used as the substrate material. Prior to plasma spray, the substrate surface was mechanically polished to #1200 grit level, cleaned and sandblasted with 450 μm SiC particles. To obtain a uniform coating, the substrate was mounted on a disk which could rotate during spraying in air using a Plasma-Technik A-3000 system (Plasma Technik A.G., Wohlen, Switzerland). The majority of coatings had a thickness in the range of 90–140 μm, except for the GHA/25BG coating with a thickness of only 45 μm.

Phases of the various coatings were analyzed by an X-ray diffractometer (Rigaku D-max IIB, Japan) operated at 30 kV and 20 mA. The microstructure/microchemistry was characterized using a scanning electron microscope (SEM) (Hitachi S-4200, Japan) equipped with an energy dispersive spectroscopy (EDS) system. The roughness of sandblasted substrate as well as the various plasma-sprayed surfaces was measured using a Surfcorder (SE-30AK Kosaka Laboratory Ltd., Japan). The measured length was 5 mm at a probe speed of 0.1 mm/s. Specimens for cross-sectional microscopy were prepared by mounting the coated specimens in epoxy resin, followed by polishing through 0.05 μm alumina.

The ASTM C633-79 method suggested for testing flame-sprayed coating bond strength was used to measure the bond strength of the present coatings. In performing this test, two identical cylindrical Ti-6Al-4V rods were prepared, one with coating on a flat surface and the other without. The flat surface of the uncoated rod, which was to be bonded to the coated rod, was sandblast-roughened to enhance resin adherence. A thin layer of bonding glue (Plasma Technik, Klebbi glue, Switzerland) was applied onto both coated and uncoated surfaces. After the two rods were carefully aligned using a special device [16], a compressive stress was applied to both rods during curing to assure an intimate contact between resin and the two surfaces. After curing at 180 °C in an oven, the bonded rods were bench cooled to room temperature. The pressure was then released and the resin-bonded rods were removed from the device. The coatings were pulled out from substrate using an Instron 8562 tester at a cross head speed of 1.0 mm/min.

A variety of synthetic solutions, such as tris-buffered and Hank's physiological solutions [17, 18], have often been used for *in vitro* biodegradation/bioactivity evaluation. In the present study, a simulated body fluid (SBF) suggested by Kokubo *et al*. [19] (Table II) was used for all immersion tests. The coated specimens, each with a surface area of 1 cm^2, were immersed in vials containing 50 ml SBF, which were maintained at 37 °C throughout

TABLE I Composition of raw HA powder used in this study

Chloride	< 0.05 wt%
Fluoride	< 0.005 wt%
Sulfate	< 0.3 wt%
Heavy metals	< 0.003 wt%
Arsenic	< 0.0002 wt%
Iron	< 0.02 wt%
Water	1.7 wt%
Assay	96.5%

Merck #2196; E.Merek, Germany.

TABLE II Composition of simulated body fluid used in this study

Constituent	g/L
NaCl	7.9949
$NaHCO_3$	0.3528
KCl	0.2235
K_2HPO_4	0.1470
$MgCl_26H_2O$	0.3050
$CaCl_2$	0.2775
Na_2SO_4	0.0710

tests. The solution was agitated daily to help maintain uniform ion, concentrations. After 30 days of immersion, the specimens were removed from the vials and stored in a desiccator for characterization.

3. Results and discussion

3.1. Characterization of HA and HA/BG powders

The morphologies of in-house fabricated BG powder, sinter-granulated monolithic HA powder, as well as a series of sinter-granulated HA/BG powders are shown in Fig. 1. As shown in the SEM micrographs, the BG powder and sinter-granulated monolithic HA (GHA) powder were irregularly shaped and dense. As mentioned earlier, both sinter-granulated HA and in-house fabricated BG powders were sieved to obtain particle sizes 44–149 μm. Among all granulated HA/BG powders, the powder containing 2.5 wt % BG (GHA/2.5BG) had the smoothest and densest structure, similar to the GHA powder, due to its small BG content. When 5 wt % BG was added in HA (GHA/5BG), however, the powder became highly porous. The majority of the pores had sizes smaller than 10 μm. Kangasmiemi *et al.* [14] attributed the BG-induced formation of porosity to the release of hydroxyl group from HA. Wang *et al.* [20] recently confirmed that the presence of BG not only enhanced the breakdown process of hydroxyl group, but also enhanced the decomposition of HA structure.

When 10 wt % BG was added (GHA/10BG), the powder surface pores became larger in size, but smaller in number. Higher magnification examination revealed many microcracks on the surface. It seems that at least two factors, i.e., BG-enhanced release of hydroxyl group and BG-induced liquid phase sintering effect [21], were operating competitively to determine the eventual porosity level of the sinter-granulated HA/BG powders. The formation of the microcracks might be explained by the differences in density and coefficient of thermal expansion (CTE) among the various phases that involved phase transformations at high temperatures (more will be discussed in a later section). When BG content was further increased to 25 wt % (GHA/25BG), numerous fine particles (mostly < 5 μm) were observed to loosely attach to the rough surface of the powder. This insufficient sintering/bonding, that caused a portion of GHA/25BG powder to disperse during plasma spraying, should be responsible for the much smaller thickness of this coating than all others, as mentioned earlier in Materials and Methods.

X-ray diffraction (XRD) patterns of the various powders are shown in Fig. 2. Even when as low as 2.5 wt % BG was added, in HA (GHA/2.5BG), the decomposition of apatite into β-TCP and α-TCP phases was readily detected. When 5 wt % BG was added (GHA/5BG), the transformed phases, particularly β-TCP, became quite significant. Such phases as $CaSiO_3$ and $Ca_4P_2O_9$ (TTCP) were also found in GHA/5BG and GHA/10BG powders. As BG content increased, the apatite intensity decreased, while the intensities of α-TCP, β-TCP, $CaSiO_3$ and $Ca_4P_2O_9$ phases increased. It was suggested [13, 14] that, when an HA/BG mixture was sintered at elevated temperatures, the sodium ions in BG might diffuse into the HA structure, causing release of a portion of hydroxyl group from HA. The HA structure with deficient hydroxyl group was less stable at high temperatures and had greater tendency to decompose and react with BG. The present results seems compatible with this theory.

When BG content was increased to 25 wt % (GHA/25BG), the apatite peaks were no longer observed.

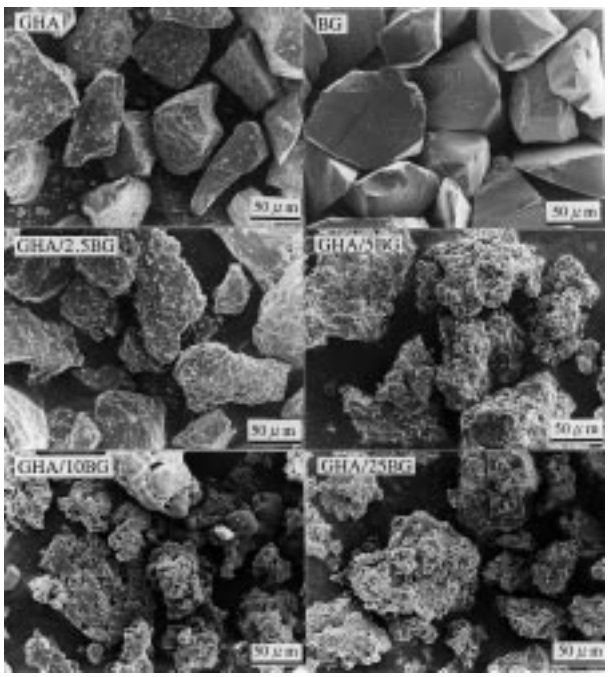

Figure 1 SEM micrographs of various powders fabricated in-house for plasma spray.

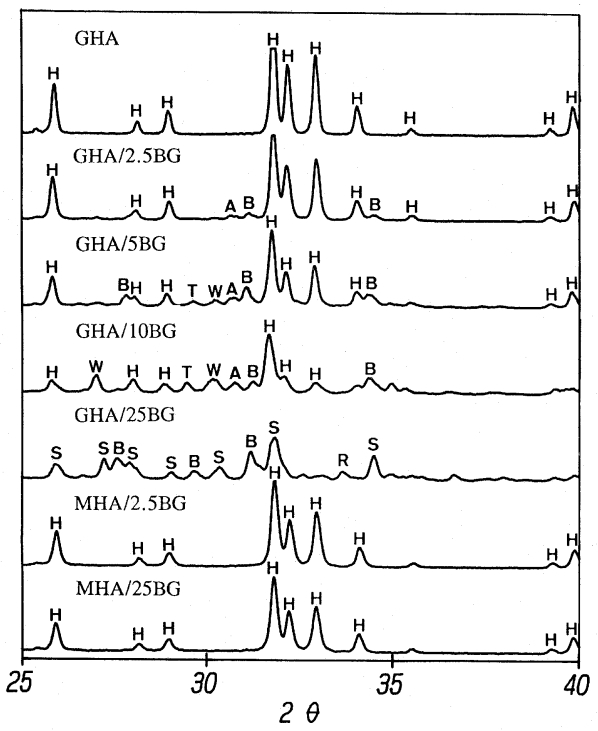

Figure 2 XRD patterns of various powders for plasma spray. (H: apatite; T: TTCP; A: α-TCP; B: β-TCP; W: $CaSiO_3$; S: $Ca_5(PO_4)_2SiO_4$; R: $\beta - NaCaPO_4$).

Instead, such phases as $Ca_5(PO_4)_2SiO_4$ and β-TCP were dominant. The XRD patterns of MHA/2.5BG and MHA/25BG powders showed no other significant phases than apatite due to their direct mixing process. As expected, there existed no characteristic diffraction peaks of BG due to its amorphous structure.

3.2. Surface roughness and bond strength of HA and HA/BG coatings

Listed in Table III are surface roughness and bond strength values of monolithic HA and the various HA/BG coatings. As indicated in the table, the surfaces of all coatings were at least twice as rough as that of initial sandblasted Ti-6Al-4V substrate. Although MHA/25BG coating surface was rougher (Ra $= 9.7\,\mu m$) than all other coating surfaces (7.6–8.5 μm), their differences were not significant.

Although the ASTM C633 method has often been used for measuring the bond strength of HA coatings, whether the measured bond strength values using this method could represent ''true'' bond strengths is still in debate [22–25]. For example, it was argued [22] that, during press-curing, the bonding resin might infiltrate through open porosity into coating interior, introducing uncertainties to the measured values. Another difficulty arises from the determination of the ''true'' fracture area. Post-test observations indicated that all major fractures of the present coated specimens occurred within coating interior. Generally only small portions of coatings were pulled out right from substrate surface. The major portions of the coatings were still bonded to the substrate when the coatings were pulled out. For simplicity, in this study, the original cross-sectional area of Ti-6Al-4V substrate was used at all times in the calculation of bond strengths.

Compared to reported values [1, 3, 24] reasonably high bond strengths were obtained from all present coatings (majority in the range 50–60 MPa). The monolithic HA coating had the highest bond strength (63.6 MPa). When BG was added in HA, the bond strength decreased more or less. This decrease in bond strength might be explained by the more porous structure of HA/BG coatings, as will be discussed in more detail in the following section. The granulated type HA/BG coatings showed no significant differences in bond strength from the mixed type HA/BG coatings. For example, GHA/25BG coating had a bond strength of 55.5 MPa, which is close to that of MHA/25BG coating, 54.6 MPa.

TABLE III Average bond strength and surface roughness of plasma-sprayed HA and HA/BG coatings

Coating	Avg. bond strength (MPa) (no. of tests = 10)	Ra (μm) (no. of tests = 5)
GHA	63.6 ± 9.1	7.6 ± 0.3
GHA/2.5BG	56.5 ± 8.0	8.4 ± 0.8
GHA/5BG	56.7 ± 1.6	8.5 ± 0.3
GHA/10BG	49.6 ± 4.8	8.5 ± 0.8
GHA/25BG	55.5 ± 5.2	7.6 ± 0.3
MHA/2.5BG	59.1 ± 3.8	8.3 ± 0.7
MHA/25BG	54.6 ± 6.1	9.7 ± 0.3
Ti6A14V substrate		3.6 ± 0.2

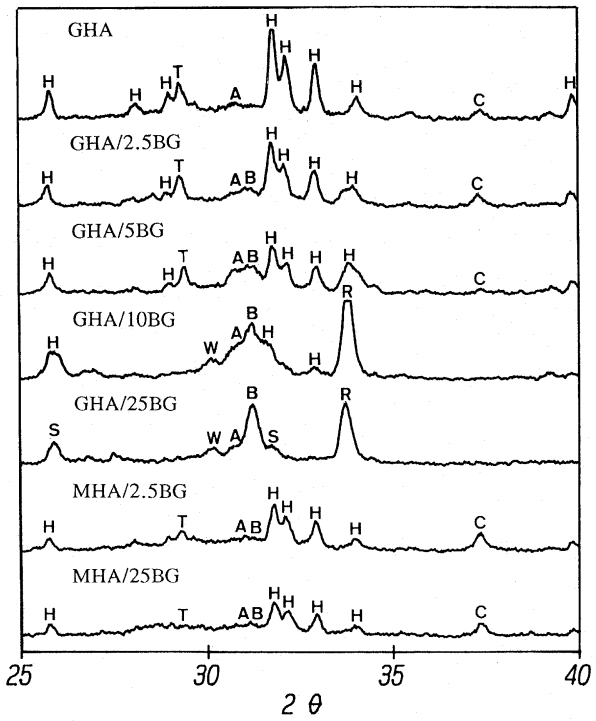

Figure 3 XRD patterns of various plasma-sprayed coatings. (H: apatite; T: TTCP; C: CaO; A: α-TCP; B: β-TCP; W: $CaSiO_3$; S: $Ca_5(PO_4)_2SiO_4$; R: $\beta - NaCaPO_4$).

3.3. Characterization of HA and HA/BG coatings

As shown in the XRD patterns in Fig. 3, the plasma-sprayed coatings generally had lower apatite crystallinity than their respective initial powders, in agreement with previous studies [16]. In addition to the broadening of apatite peaks, $Ca_4P_2O_9$ (TTCP), CaO and α-TCP (might be overlapped with low intensity β-TCP) phases were observed in monolithic HA and GHA/2.5BG coatings. The high temperature involved in plasma spray process had obviously enhanced the decomposition of apatite as well as chemical reactions between different phases. In GHA/5BG coating, the intensities of α-TCP and β-TCP continued to increase at the expense of the apatite phase. The CaO intensity became very low. In GHA/10BG coating, the TTCP phase disappeared, while $\beta - NaCaPO_4$ became dominant. The formation of $\beta - NaCaPO_4$ as a result of the reaction between apatite and sodium ions in glass was observed previously by Kangasniemi *et al.* [14]. The β-TCP intensity also largely increased as a result of high temperature decomposition of apatite [12, 20]. As BG content increased to 25 wt %, the β-TCP intensity further increased at the expense of $\beta - NaCaPO_4$ and other minor phases. As a result, these two phases became almost equally dominant. The $Ca_5(PO_4)_2SiO_4$ phase, which had the highest intensity in the initial GHA/25BG powder, was also decomposed during the plasma spray process.

The XRD patterns of MHA/2.5BG and MHA/25BG coatings were similar to that of GHA/2.5BG coating. The apatite phase largely lost its crystallinity, while CaO, TTCP as well as small amounts of α-TCP and β-TCP were induced. Again, the presence of BG has enhanced the decomposition of HA during plasma spraying.

SEM micrographs of the series of coatings are given in

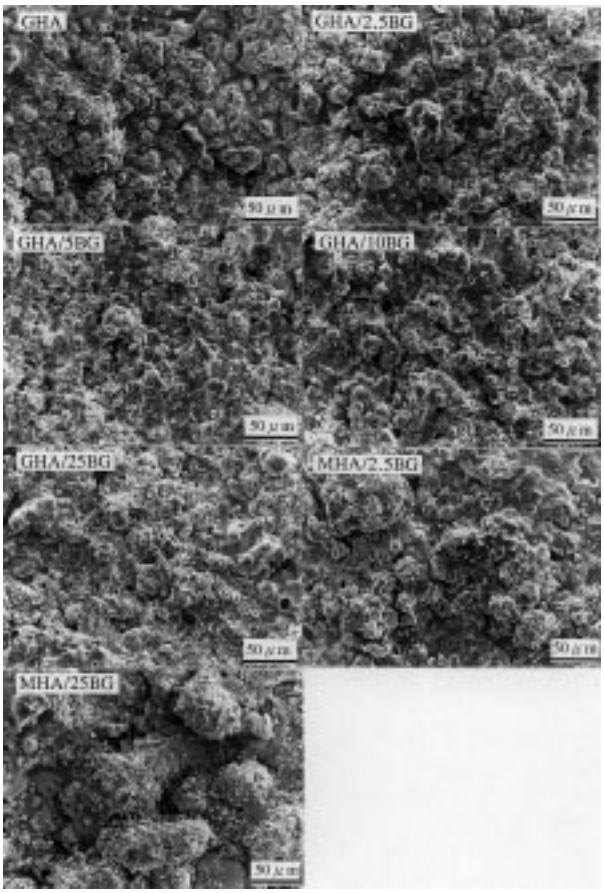

Figure 4 SEM micrographs of various plasma-sprayed coatings.

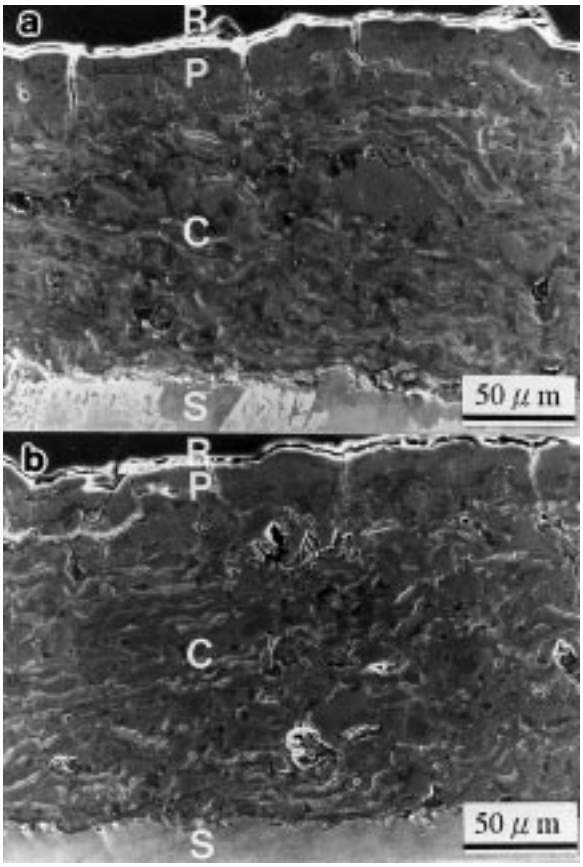

Figure 5 Cross-sectional SEM micrographs of plasma-sprayed MHA/2.5BG (a) and GHA/2.5BG (b) coatings after immersion in SBF for 30 days. (S: substrate; C: plasma-sprayed coating; P: precipitated apatite; R: mounting resin).

Fig. 4. Similar to that observed earlier [16], patches of smooth and shiny glassy film and irregularly-shaped particles were observed on the surface of HA coating. In their transmission electron microscopic (TEM) study, Ji *et al*. [26] showed that the plasma spray-induced glassy structure was an amorphous form of calcium phosphate. During plasma spraying, small size powder was completely melted, while larger size powder, such as the one used in the present study, was only partially melted resulting in a coating morphology comprising the observed irregularly-shaped particles [24, 27]. This observation is consistent with the earlier-discussed XRD results (e.g. broadening in apatite peaks).

Surface morphology of all sinter-granulated type coatings was similar to that of monolithic HA coating. The MHA/2.5BG coating also had a similar surface morphology due to the small BG content. The MHA/25BG coating, however, had a quite different morphology. Bubbles and irregularly-shaped particles were observed on the coating surface. The presence of the large bubbles (could be larger than 50 μm) caused this coating surface to be rougher than others. The mechanism of formation of this structure was described elsewhere [16].

3.4. Immersion behavior of HA and HA/BG coatings

When immersed in SBF solution, dissolution and apatite precipitation could both occur to the plasma-sprayed coatings. At the early stage, the dissolution of mixed type coatings generally proceeded faster than precipitation, causing the plasma-sprayed coating thickness to decrease. When the precipitation process picked up its speed and eventually formed an apatite layer that effectively ''sealed'' the underneath plasma-sprayed coating, the dissolution of plasma-sprayed coating virtually stopped. The granulated type coatings dissolved little, if any, before the apatite precipitation process became dominant. Fig. 5 serves as an example for demonstration of these phenomena. The as-plasma-sprayed MHA/2.5BG coating had an average thickness of 138.5 μm. After immersion in SBF for 30 days, its thickness decreased to 114.0 μm, while the precipitated apatite layer grew to a thickness of 30.0 μm (Fig. 5a). The immersed plasma-sprayed GHA/2.5BG coating, however, virtually did not dissolve in the SBF, while the precipitated apatite layer grew to a thickness of 28.4 μm (Fig. 5b).

The plasma-sprayed coating could be easily distinguished from the precipitated apatite layer due to their morphological differences. The precipitated apatite layer was smoother and denser than the plasma-sprayed coating. Cracks, that were essentially perpendicular to the coating surface and possibly formed as a result of the drying process, were present in the precipitated layer. Most of the cracks terminated at the interface between plasma-sprayed coating and precipitated layer. In contrast, the typical plasma spray-induced flake type structural imperfections within coatings were running roughly parallel to the coating surface.

The XRD patterns in Fig. 6 confirmed that the

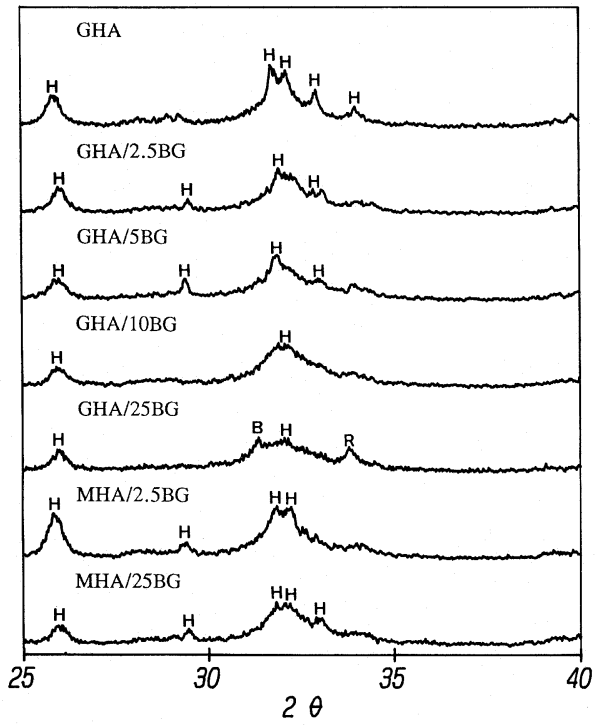

Figure 6 XRD patterns of various plasma-sprayed coatings after immersion in SBF for 30 days. (H: apatite; B: β-TCP; R: $\beta - NaCaPO_4$).

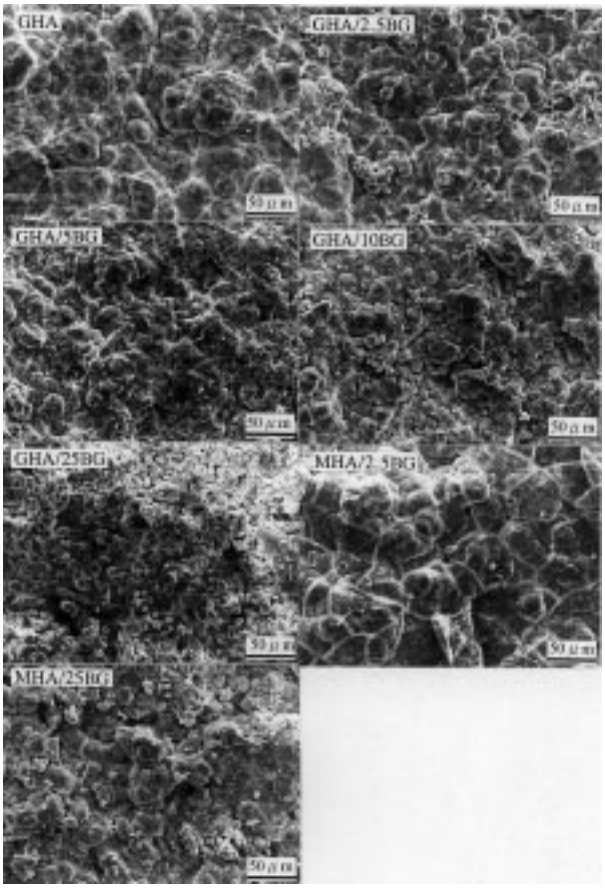

Figure 7 SEM micrographs of various plasma-sprayed coatings after immersion in SBF for 30 days.

precipitated layer formed on all immersed coating surfaces primarily had an apatite structure, though with lower crystallinity. CaO and other minor phases, that were present in as-sprayed coatings, did not exist in the precipitated layer. The XRD pattern of the immersed GHA/25BG coating showed that $\beta - NaCaPO_4$, and β-TCP intensities were still significant probably due to the small thickness of the precipitated layer that allowed the underneath plasma-sprayed coating (dominated with $\beta - NaCaPO_4$, and β-TCP phases) to have also been detected.

From the broad face SEM micrographs (Fig. 7), it can be seen that the apatite precipitated on all coatings had similar morphology, except for that precipitated on monolithic HA coating and the coatings containing 2.5 wt % BG (GHA/2.5BG and MHA/2.5BG coatings). The glassy phase and numerous irregularly-shaped small particles on the surfaces of as-sprayed coatings were no longer present. Instead, the surface of the precipitated apatite layer was covered with clusters of spherulites. Higher magnification examination revealed that most of the spherulites had sizes of several microns. The cracks observed in the precipitated apatite cross sections were again observed in the broad face micrographs of all precipitated apatite surfaces.

To further confirm that the observed apatite layer was indeed precipitated from the SBF solution, a series of SEM/EDS point analyses were performed on the cross sections of immersed GHA/10BG coating. As shown in Fig. 8, both Ca/P and Si/P ratios of the immersed coating started to increase from a depth between 20 and 25 μm from surface, consistent with the measured precipitation thickness of 22.6 μm. Since Si was present in the plasma-sprayed coating but not in the initial SBF solution or apatite, the marked difference in Si/P ratio between spots #4 and #5 in Fig. 8c indicates that the interface between precipitated apatite layer and plasma-sprayed coating is somewhere between these two spots.

The average dissolution depth and apatite precipitation thickness of the series of coating systems are compiled in Table IV. The majority of the thickness of precipitated layer was in the range of 20–30 μm, except for that on the immersed GHA/25BG coating (only 11.9 μm). Nevertheless, all the coatings showed a strong tendency for ''attracting'' apatite precipitate onto their surfaces. The reason for the much lower apatite precipitation rate on GHA/25BG coating was possibly due to the lack of apatite phase in its as-sprayed coating.

The dissolution rate in SBF of a coating is practically important, since it could be an indication for the *in vivo* bioresorption/biodegradation rate of the coating [28, 29], especially when thinner coatings are pursued. The biodegradation phenomenon of HA in both *in vitro* and animal studies has been reported by Ramselaar *et al.* [30], Blitterswijk *et al.* [31], and others [32–34]. It was also reported that higher crystallinity HA coating resulted in less resorption rate [9, 29], and the presence of such phases as β-TCP and TTCP would enhance the resorption process of HA coating [35].

In the present study, the dissolution depth of plasma-sprayed coatings was found to depend largely on the type and composition of the coating. Though not fully understood, it is surprisingly interesting to note that granulated type HA/BG coatings were much less dissolvable in SBF than monolithic HA or mixed type HA/BG coatings. The monolithic HA coating, that had

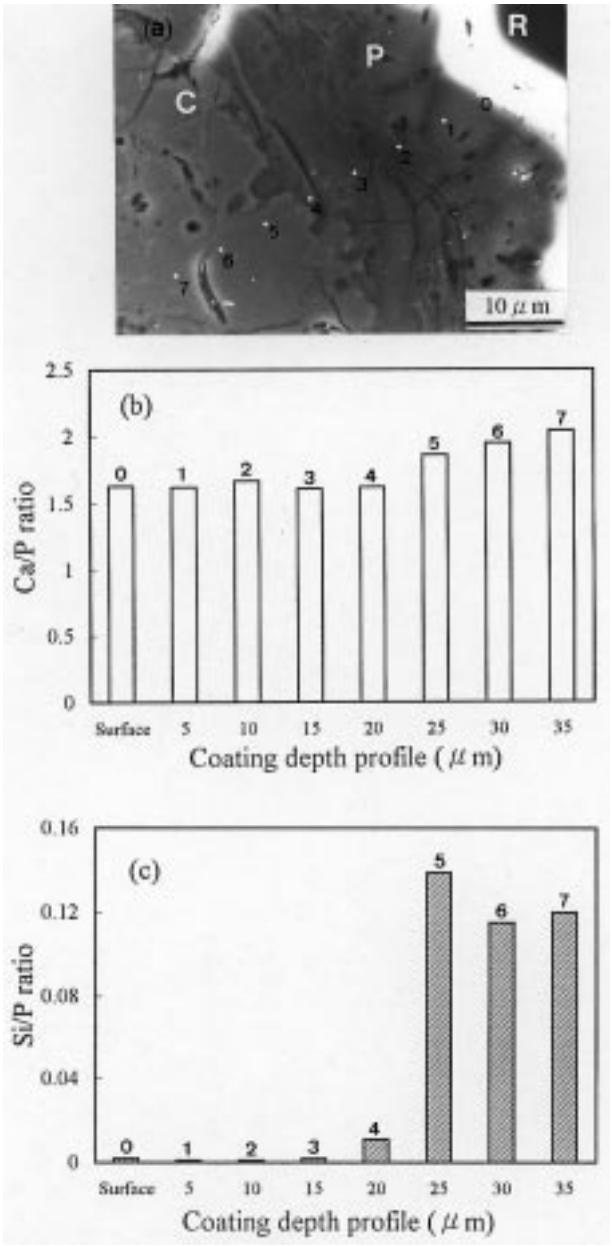

Figure 8 Cross-sectional SEM micrograph (a) and EDS point analyses (b, c) of GHA/10BG coating immersed in SBF for 30 days. (C: plasma-sprayed coating; P: precipitated apatite; R: mounting resin).

TABLE IV Dissolution depth of plasma-sprayed coating and precipitated apatite thickness

Coating	Precipitated apatite thickness (μm) (no. of measurements = 20)	Dissolution depth of plasma-sprayed coating (μm)
GHA	19.5 ± 5.5	34.5
GHA/2.5BG	28.4 ± 6.1	nil
GHA/5BG	23.1 ± 6.8	nil
GHA/10BG	22.6 ± 6.1	5.6
GHA/25BG	11.9 ± 4.0	nil
MHA/2.5BG	30.0 ± 7.1	24.5
MHA/25BG	23.3 ± 7.7	22.8

the highest apatite crystallinity, dissolved most seriously (34.5 μm). The mixed type MHA/2.5BG and MHA/25BG coatings were the second dissolvable (with dissolution depths of 24.5 and 22.8 μm, respectively). All granulated HA/BG coatings had more non-apatite phases than that of monolithic HA coating. However, all these HA/BG coatings virtually did not dissolve, except for the GHA/10BG coating with a relatively thin (5.6 μm) depth of dissolution. It seems that the presently used granulation method for the preparation of HA/BG powders plays a predominant role in determining the dissolution behavior of plasma-sprayed coatings.

4. Conclusions

1. The in-house fabricated BG and sinter-granulated HA powders were irregularly shaped and dense. When 5 wt % or more BG was added in HA, the powder became rough and porous. XRD patterns showed that the presence of BG enhanced the decomposition of HA structure during fabrication of the powders. As BG content increased, the apatite intensity decreased, while the intensities of α-TCP, β-TCP, $CaSiO_3$ and $Ca_4P_2O_9$ phases increased.

2. The surfaces of all coatings were at least twice as rough as that of initial sandblasted substrate. The MHA/25BG coating surface was the roughest among all.

3. Reasonably high bond strengths were obtained from all coatings. The granulated type HA/BG coatings showed no significant differences in bond strength from the mixed type HA/BG coatings.

4. The plasma-sprayed coatings had lower apatite crystallinity than their respective initial powders. The plasma spray process itself and the presence of BG enhanced the decomposition of apatite. As BG content increased, the relative amounts of such phases as TCP and $\beta - NaCaPO_4$ increased at the expense of apatite.

5. Surface morphology of all sinter-granulated type coatings was similar to that of monolithic HA coating, that was composed of patches of smooth and shiny glassy film and irregularly-shaped particles on its surface. Bubbles and irregularly-shaped particles were observed on the MHA/25BG coating surface.

6. The dissolution depth of plasma-sprayed coatings immersed in SBF was largely dependent on the type and composition of the coating. Granulated type HA/BG coatings were much less dissolvable than monolithic HA or mixed type HA/BG coatings. It seems that the presently used granulation method for the preparation of HA/BG powders plays a predominant role in determining the dissolution behavior of plasma-sprayed coatings.

Acknowledgments

The authors acknowledge with appreciation the support for this research by the National Science Council of the Republic of China under the contract No. NSC 84-2213-E-006-121 & 122 & 123.

References

1. R. G. T. GEESINK, K. DE GROOT and C. P. A. T. KLEIN, *Clin. Orthop.* **225** (1987) 147.
2. J. E. LEMONS, *ibid.* **235** (1988) 220.

3. K. A. THOMAS, *Orthopaedics* **17** (1994) 267.
4. W. R. LACEFIELD, in ''Bioceramics: Material Characteristics Versus *in vivo* Behavior'', edited by P. Ducheyne and J. E. Lemons. *Ann. N. Y. Acad. Sci.* **523** (1982) 72.
5. S. MARUNO, K. HAYASHI, Y. SUMI, Y. F. WANG and H. IWATA, in ''Handbook of Bioactive Ceramics'', Vol. II, edited by T. Yamamuro, L. L. Hench and J. Wilson (CRC Press, Boca Raton, FL, 1990) p. 187.
6. C. S. KIM and P. DUCHEYNE, *Biomaterials* **12** (1991) 461.
7. E. RUCKENSTEIN, S. GOURISANKAR and R. E. BAIER, *J. Colloid Interface Sci.* **96** (1983) 245.
8. C. K. WANG, J. H. CHERN LIN, C. P. JU, H. C. ONG and R. P. H. CHANG, *Biomaterials* **18** (1997) 1331.
9. S. H. MAXIAN, J. P. ZAWADSKY and M. G. DUNN, *J. Biomed. Mater. Res.* **27** (1993) 111.
10. L. L. HENCH, in ''Handbook of Bioactive Ceramics'', Vol. I. edited by T. Yamamuro, L. L. Hench and J. Wilson (CRC Press, Boca Raton, FL, 1990) p. 7.
11. M. MOCHIDA, T. FUJIL and M. OGINO, *J. Ceram. Soc. Jpn. Int. Ed.* **95** (1987) 751.
12. J. C. KNOWLES and W. BONFIELD, *J. Biomed. Mater. Res.* **27** (1993) 1591.
13. J. D. SANTOS, J C. KNOWLES, R. L. REIS, F. J. MONTEIRO and G. W. HASTINGS, *Biomaterials* **15** (1994) 5.
14. I. M. O. KANGASNIEMI, K. DE GROOT, J. WOLKE, Ö. ANDERSSON, Z. LUKLINSKA, J. G. M. BECHT, M. LAKKISTO and A. YLI-URPO, *J. Mater. Sci. Mater. Med.* **2** (1991) 133.
15. J. H. CHERN LIN, M. L. LIU and C. P. JU, *Dent. Mater.* **9** (1993) 286.
16. *Idem.*, *J. Mater. Sci. Mater. Med.* **5** (1994) 279.
17. *Idem.*, *J. Biomed. Mater. Res.* **28** (1994) 723.
18. C. Y. KIM, A. E. CLARK and L. L. HENCH, *J. Non-Cryst. Solids* **113** (1989) 195.
19. S. CHO, K. NAKANISHI, T. KOKUBO, N. SOGA, C. OHTSUKI, T. NAKAMURA, T. KITSUGI and T. YAMAMURO, *J. Amer. Ceram. Soc.* **78** (1995) 1769.
20. C. K. WANG, J. H. CHERN LIN and C. P. JU, *Mater Chem. Phy.* **53** (1997) 138.
21. J. D. SANTOS, R. L. REIS, F. J. MONTEIRO, J. C. KNOWLES and G. W. HASTING, *J. Mater. Sci. Mater. Med.* **6** (1995) 348.
22. K. DE GROOT, C. P. A. T. KLEIN, J. G. C. WOLKE and J. M. A. DE BLIECK-HOGERVORST, in ''Handbook of Bioactive Ceramics'', Vol. II, edited by T. Yamamuro, L. L. Hench and J. Wilson (CRC Press, Boca Raton, FL, 1990) p. 133.
23. M. J. FILIAGGI, N. A. COOMBS and R. M. PILLIAR, *J. Biomed. Mater. Res.* **22** (1991) 1211.
24. J. G. C. WOLKE, C. P. A. T. KLEIN and K. DE GROOT, in ''Bioceramics and the Human Body'', edited by A. Ravaglioli and A. Krajewski (Elsevier, London, England, 1992) p. 166.
25. S. J. YANKEE, B. J. PLETKA, R. L. SALSBURY and W. A. JOHNSON, in ''Surface Modification Technologies IV'', edited by T. S. Sudarshan, D. G. Bhat and M. Jeandin (TMS, Warrendale, Pennsylvania, 1991) p. 261.
26. H. JI, C. B. PONTON and P. M. MARQUIS, *J. Mater. Sci. Mater. Med.* **3** (1992) 283.
27. W. TONG, J. CHEN, X. LI, Y. CAO, Z. YANG, J. FENG and X. ZHANG, *Biomaterials* **17** (1996) 1507.
28. P. DUCHEYNE, S. RADIN and L. KING, *J Biomed. Mater. Res.* **27** (1993) 25.
29. C. P. A. T. KLEIN, J. G. C. WOLKE, J. M. A. DE BLIECK-HOGERVORST and K. DE GROOT, *ibid.* **28** (1994) 961.
30. M. M. A. RAMSELAAR, F. C. M. DRIESSENS, W. KALK, J. D. DE WIJN and P. J. VAN MULLEN, *J. Mater. Sci. Mater. Med.* **2** (1991) 63.
31. C. A. VAN BLITTERSWIJK, J. J. GROTE, W. KUIJPERS, W. TH. DAEMS and K. DE GROOT, *Biomaterials* **7** (1986) 137.
32. R. L. REIS and F. J. MONTEIRO, *J. Mater. Sci. Mater. Med.* **7** (1996) 407.
33. C. Y. YANG, R. M. LIN, B. C. WANG, T. M. LEE, E. CHANG,